Enhancing Low Electronic Conductivity Materials in All Active Material Electrodes through Multicomponent Architecture

Supporting Information

Chen Cai, Gary Koenig

Chen Cai[a], Gary M. Koenig Jr.[a]*

[a]Department of Chemical Engineering, University of Virginia, 102 Engineers Way, Charlottesville, 22904-4741, VA, USA.

*Corresponding author

GMK: gary.koenig@virginia.edu; Phone +1 (434) 982-2714; Fax +1 (434) 982-2658;

Department of Chemical Engineering, University of Virginia, 102 Engineers' Way P.O. Box 400741, Charlottesville, VA 22904, USA

Model Description

The model is a pseudo-two-dimensional (P2D) implicit numerical framework, originally proposed by Newman et al. [1–3]. The following are the governing equations used this work:

For Pure LNMO AAM Cathode Cell:

Electrolyte Concentration:

$$\epsilon_E \frac{\partial c_E}{\partial t} = \frac{\partial}{\partial x}\left(D_{eff}(c_E)\frac{\partial c_E}{\partial x}\right) + A_{LNMO} j_{LNMO}\left(1 - t_+^0\right)$$

Electrode Potential:

$$\frac{\partial \phi_1}{\partial x} = \frac{-i_1}{\sigma_{eff}(c_{LNMO})}$$

Electrolyte Potential:

$$\frac{\partial \phi_2}{\partial x} = -\frac{i_2}{\kappa_{eff}(c)} + \frac{2RT}{F}\left(1 + \frac{\partial \ln f_{\pm}(c_E)}{\partial \ln c_E}\right)\left(1 - t_+^0\right)\frac{\partial \ln c_E}{\partial x}$$

Lithium Flux Kinetics:

$$j_{LNMO} = -2k_{LNMO} c_E^{0.5}\left(c_{LNMO}^{surface}\right)^{0.5}\left(c_{LNMO}^{surface} - c_{LNMO,max}^{surface}\right)^{0.5} Sinh\left(\frac{F}{RT}(\phi_1 - \phi_2 - U_{LNMO})\right)$$

Lithium Flux across Electrode & Electrolyte Interface:

$$j_{LNMO} = -D_{LNMO}\frac{\partial c_{LNMO}^{surface}}{\partial r}$$

Electrolyte Current:

$$A_{LNMO} j_{LNMO} = -\frac{1}{F}\frac{\partial i_2}{\partial x}$$

Conservation of Current:

$$I = i_1 + i_2$$

Volumetric Surface Area:

$$A_{LNMO} = \frac{3}{R_{LNMO}}\epsilon_{LNMO}$$

Electrode Particle Concentration:

$$\frac{\partial c_{LNMO}}{\partial t} = D_{LNMO}\left(\frac{1}{r^2}\frac{\partial}{\partial r}\left(r^2\frac{\partial c_{LNMO}}{\partial r}\right)\right)$$

Effective Ionic Conductivity and Diffusivity:

$$\frac{\kappa_{eff}(c_E)}{\kappa(c_E)} = \frac{D_{eff}(c_E)}{D(c_E)} = \epsilon_E^{\alpha}$$

Effective Electronic Conductivity:

$$\sigma_{eff}(c_{LCO}, c_{LNMO}) = \sigma_{LNMO}\epsilon_{LNMO}^{\alpha}$$

For Blended 45%LCO AAM Cathode Cell:

Electrolyte Concentration:

$$\epsilon_E \frac{\partial c_E}{\partial t} = \frac{\partial}{\partial x}\left(D_{eff}(c_E)\frac{\partial c_E}{\partial x}\right) + (A_{LCO} j_{LCO} + A_{LNMO} j_{LNMO})\left(1 - t_+^0\right)$$

Electrode Potential:

$$\frac{\partial \phi_1}{\partial x} = \frac{-i_1}{\sigma_{eff}(c_{LCO}, c_{LNMO})}$$

Electrolyte Potential:

$$\frac{\partial \phi_2}{\partial x} = -\frac{i_2}{\kappa_{eff}(c)} + \frac{2RT}{F}\left(1 + \frac{\partial \ln f_{\pm}(c_E)}{\partial \ln c_E}\right)\left(1 - t_+^0\right)\frac{\partial \ln c_E}{\partial x}$$

Lithium Flux Kinetics:

$$j_{LCO} = -2k_{LCO} c_E^{0.5}\left(c_{LCO}^{surface}\right)^{0.5}\left(c_{LCO}^{surface} - c_{LCO,max}^{surface}\right)^{0.5} Sinh\left(\frac{F}{RT}(\phi_1 - \phi_2 - U_{LCO})\right)$$

$$j_{LNMO} = -2k_{LNMO} c_E^{0.5}\left(c_{LNMO}^{surface}\right)^{0.5}\left(c_{LNMO}^{surface} - c_{LNMO,max}^{surface}\right)^{0.5} Sinh\left(\frac{F}{RT}(\phi_1 - \phi_2 - U_{LNMO})\right)$$

Lithium Flux across Electrode & Electrolyte Interface:

$$j_{LCO} = -D_{LCO}\frac{\partial c_{LCO}^{surface}}{\partial r}$$

$$j_{LNMO} = -D_{LNMO}\frac{\partial c_{LNMO}^{surface}}{\partial r}$$

Electrolyte Current:

$$A_{LCO} j_{LCO} + A_{LNMO} j_{LNMO} = -\frac{1}{F}\frac{\partial i_2}{\partial x}$$

Conservation of Current:

$$I = i_1 + i_2$$

Volumetric Surface Area:

$$A_{LCO} = \frac{3}{R_{LCO}}\epsilon_{LCO}$$

$$A_{LNMO} = \frac{3}{R_{LNMO}}\epsilon_{LNMO}$$

Electrode Particle Concentration:

$$\frac{\partial c_{LCO}}{\partial t} = D_{LCO}\left(\frac{1}{r^2}\frac{\partial}{\partial r}\left(r^2\frac{\partial c_{LCO}}{\partial r}\right)\right)$$

$$\frac{\partial c_{LNMO}}{\partial t} = D_{LNMO}\left(\frac{1}{r^2}\frac{\partial}{\partial r}\left(r^2\frac{\partial c_{LNMO}}{\partial r}\right)\right)$$

Effective Ionic Conductivity and Diffusivity:

$$\frac{\kappa_{eff}(c_E)}{\kappa(c_E)} = \frac{D_{eff}(c_E)}{D(c_E)} = \epsilon_E^{\alpha}$$

Effective Electronic Conductivity (Perfect Percolation Assumed):

$$\sigma_{eff}(c_{LCO}, c_{LNMO}) = \sigma_{LCO}\epsilon_{LCO}^{\alpha} + \sigma_{LNMO}\epsilon_{LNMO}^{\alpha}$$

List of Symbols	
Electronic Conductivity	σ
Ionic Conductivity	κ
Liquid Li^+ Concentration	c_E
Solid Li^+ Concentration in LCO	c_{LCO}
Solid Li^+ Concentration in LNMO	c_{LNMO}
Solid Potential	ϕ_1
Liquid Potential	ϕ_2
Volume Fraction	ε
Li^+ Intercalation	j
Open Circuit Potential	U
Discharge Current Density	I
Solid Phase Current Density	i_1
Liquid Phase Current Density	i_2
Volumetric Solid Particle Surface Area	A
LCO Solid Particle Radius	R_{LCO}
LNMO Solid Particle Radius	R_{LNMO}
Electrolyte Diffusivity	D
Solid State Diffusivity	D_s
Bruggeman Exponent	α
Transference number	t_+^0
Faraday Constant	F
Temperature	T
Gas Constant	R

Table S1. Cathode Parameters used in P2D simulations.

Parameters	$LiCoO_2$	$LiNi_{0.5}Mn_{0.5}O_2$
Solid State Li^+ Diffusivity ($m^2\ s^{-1}$)	3.5×10^{-13} [4]	1×10^{-14} [5]
Active Material Radius (m)	2.0×10^{-7}, SEM	2.3×10^{-7}, SEM
Rate Constant ($m^{2.5}\ mol^{-0.5}\ s^{-1}$)	3.1×10^{-13} [6]	7.0×10^{-14} [7]
Crystal Density ($g\ cm^{-3}$)	5.0 [8]	4.63 [9]
Electronic Conductivity ($S\ m^{-1}$)	$7000 \times (1 - x)^2 + 5 \times (1 - x) + 0.054$, $0.5 \leq x \leq 1.0$ in Li_xCoO_2 [3,10,11]	9.5×10^{-4}, Measured
Modified Conductivity ($S\ m^{-1}$)		$(1 + Tanh((0.88 - x) \times 12)) / 130 - 0.0012 \times x + 0.0011 + (-1 + Tanh((0.94 - x) \times 60)) / 5000$, $0.4 \leq x \leq 1.0$ in $Li_xNi_{0.5}Mn_{0.5}O_2$, Fitted
Open Circuit Voltage (V)	$-Tanh(5.7(x - 0.555)) - 1) / 3.1 - (Exp(59(x - 0.84) + 1) / 4000 + Tanh(7(x - 0.76) - 1) / 45 + Exp(-400(x - 0.5)) / 40 + 3.88$, $0.5 \leq x \leq 1.0$ in Li_xCoO_2 [3,12]	$Tanh(-(x - 0.295) \times 2.7) + 1 - Exp((x - 0.92) \times 90) / 1000 + 3.685$, $0.4 \leq x \leq 1.0$ In $Li_xNi_{0.5}Mn_{0.5}O_2$, Fitted

Table S2. Anode and other parameters used in P2D simulations.

Electrolyte and Other Parameters	Value
Transference number, t_+^0	0.415 [13]
Initial Concentration (mol m^{-3})	1200, Experimental
Thermodynamic Factor, $(1+\frac{\partial ln f_{\pm}}{\partial ln c})(1-t_+^0)$	$0.28687\ c^2 + 0.74678\ c + 0.44103$ [14]
Conductivity (S m^{-1})	$0.1297c^3 + 2.51c^{1.5} + 3.329c$ [14]
Diffusivity ($m^2\ s^{-1}$)	$(-6.9444c^2 + 7.3611c + 2.65) \times 10^{-10}$, $c < 0.8$, $6.4753 \times \mathrm{Exp}(-0.573c) \times 10^{-10}$, $c \geq 0.8$ [14]
Temperature (K)	298.15, Room Temperature
Gas Constant (J K^{-1} mol^{-1})	8.3145
Faraday Constant (A s mol^{-1})	96485
Separator Thickness (μm)	100, Experimental
Separator Bruggeman Exponent	5.1, Experimental
Separator Porosity	0.78, Experimental
Anode Thickness (μm)	710, Experimental
Anode Solid State Li^+ Diffusivity ($m^2\ s^{-1}$)	2.0×10^{-12} [15]
Anode Active Material Radius (m)	1.7×10^{-7} [16]
Anode Porosity	0.40, Experimental
Anode Bruggeman Exponent	1.5
Anode Rate Constant ($m^{2.5}\ mol^{-0.5}\ s^{-1}$)	3.90×10^{-13} [17]
Anode Density (kg m^{-3})	3480 [18]
Anode Capacity (mA h g^{-1})	175 [19]
Anode Variable conductivity (S m^{-1})	$300(x + 10^{-6})^{0.38} \times 5^{(y-1)} / \mathrm{Exp}(4.37(y-1)^{200})$, $0 \leq y \leq 1.0$ in $Li_{4+3y}Ti_5O_{12}$ [20]
Anode Open Circuit Voltage (V, vs Li/Li^+)	$0.21\mathrm{Exp}(-116.96y) + 0.45\mathrm{Exp}(-5000y) + 0.27706\mathrm{Exp}(-1010.1y) + 1.56 - 0.001\mathrm{Exp}(50(y-0.87))$, $0 \leq y \leq 1.0$ in $Li_{4+3y}Ti_5O_{12}$ [3,20]

Table S3. Cathode Dimensions used in P2D simulation

Parameters	0%LCO	45%LCO
Cathode Thickness (m)	5.5×10^{-4}, Measured	4.8×10^{-4}, Measured
Bruggeman Exponent	1.5	1.5
LCO Volume Fraction	0	0.27
LNMO Volume Fraction	0.59	0.36
Electrolyte Volume Fraction	0.41	0.37

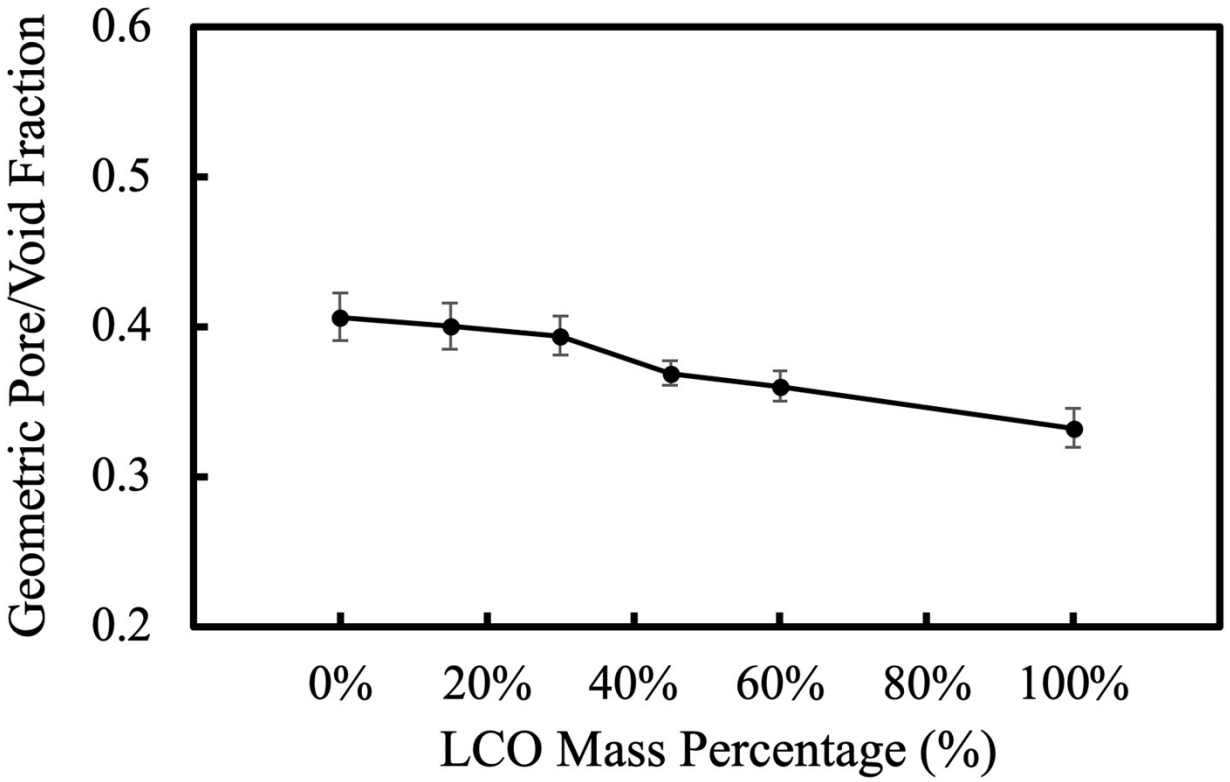

Figure S1. AAM electrode geometric pore/void fraction for the different mass loadings of LCO blended with LNMO. Error bars are the standard deviations of the mean of 3 independent experimental measurements on electrode pellets.

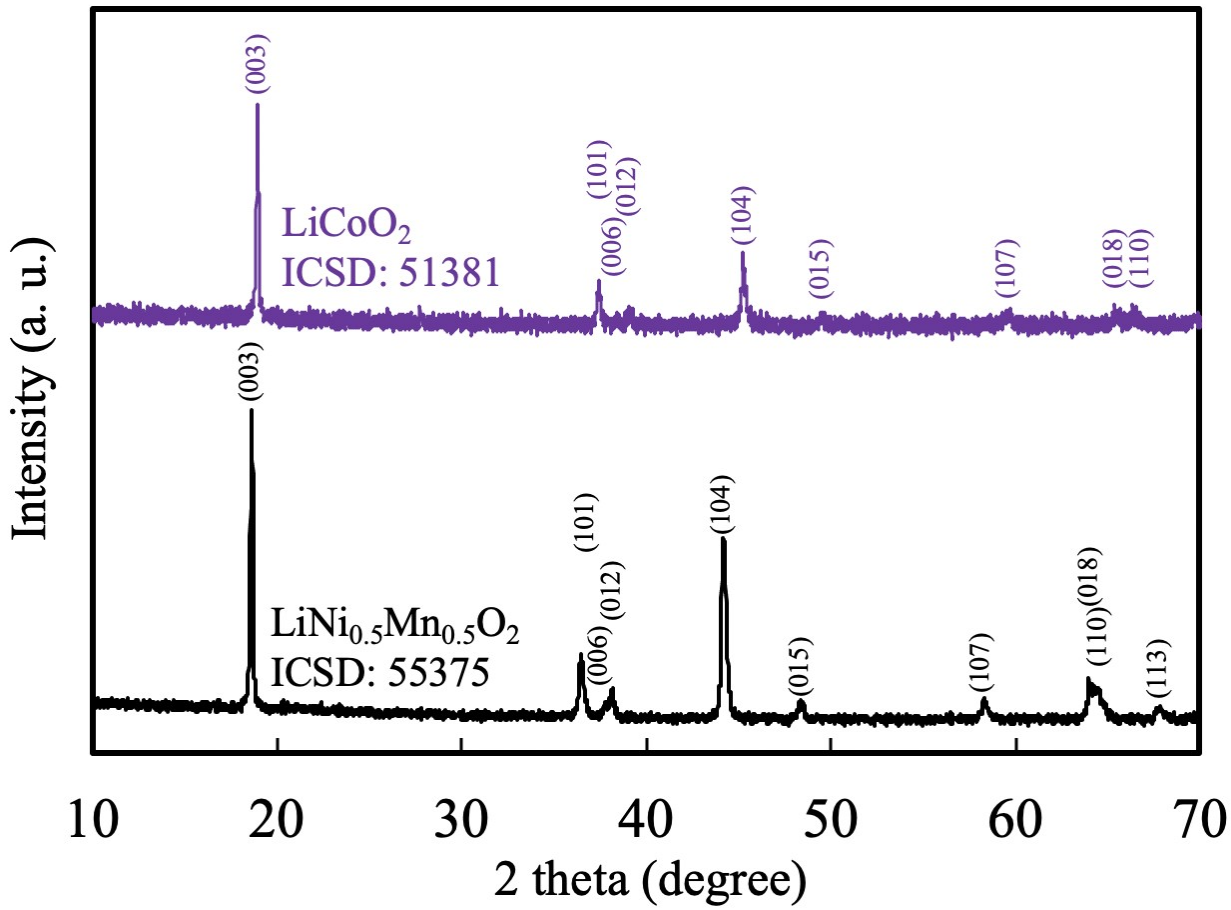

Figure S2. XRD patterns for synthesized powders of LCO (purple) and LNMO (black) [21,22].

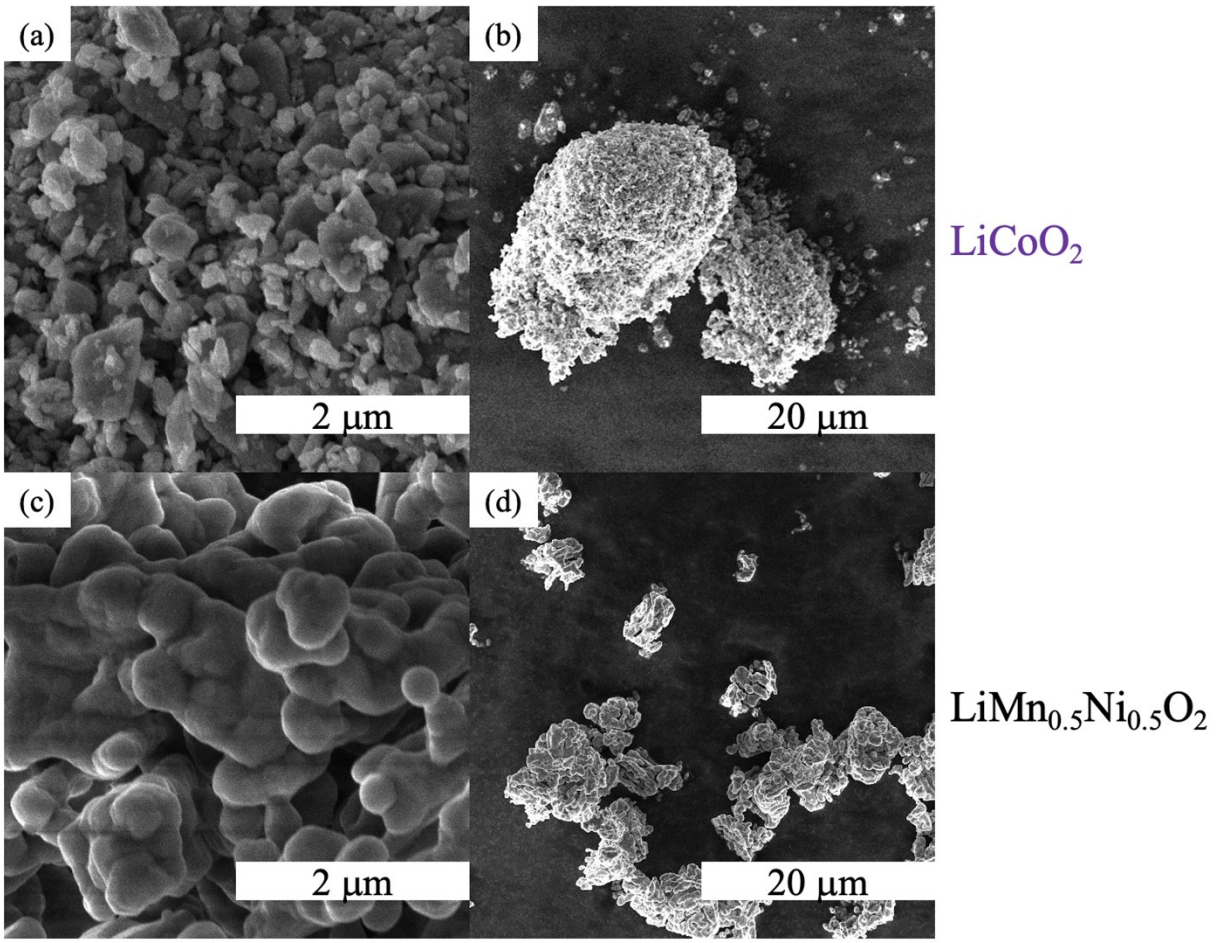

Figure S3. SEM images for the synthesized powders of (a, b) $LiCoO_2$ (LCO) and (c, d) $LiNi_{0.5}Mn_{0.5}O_2$ (LNMO). The images in (b) and (d) are lower magnification of the same samples imaged in (a) and (c), respectively.

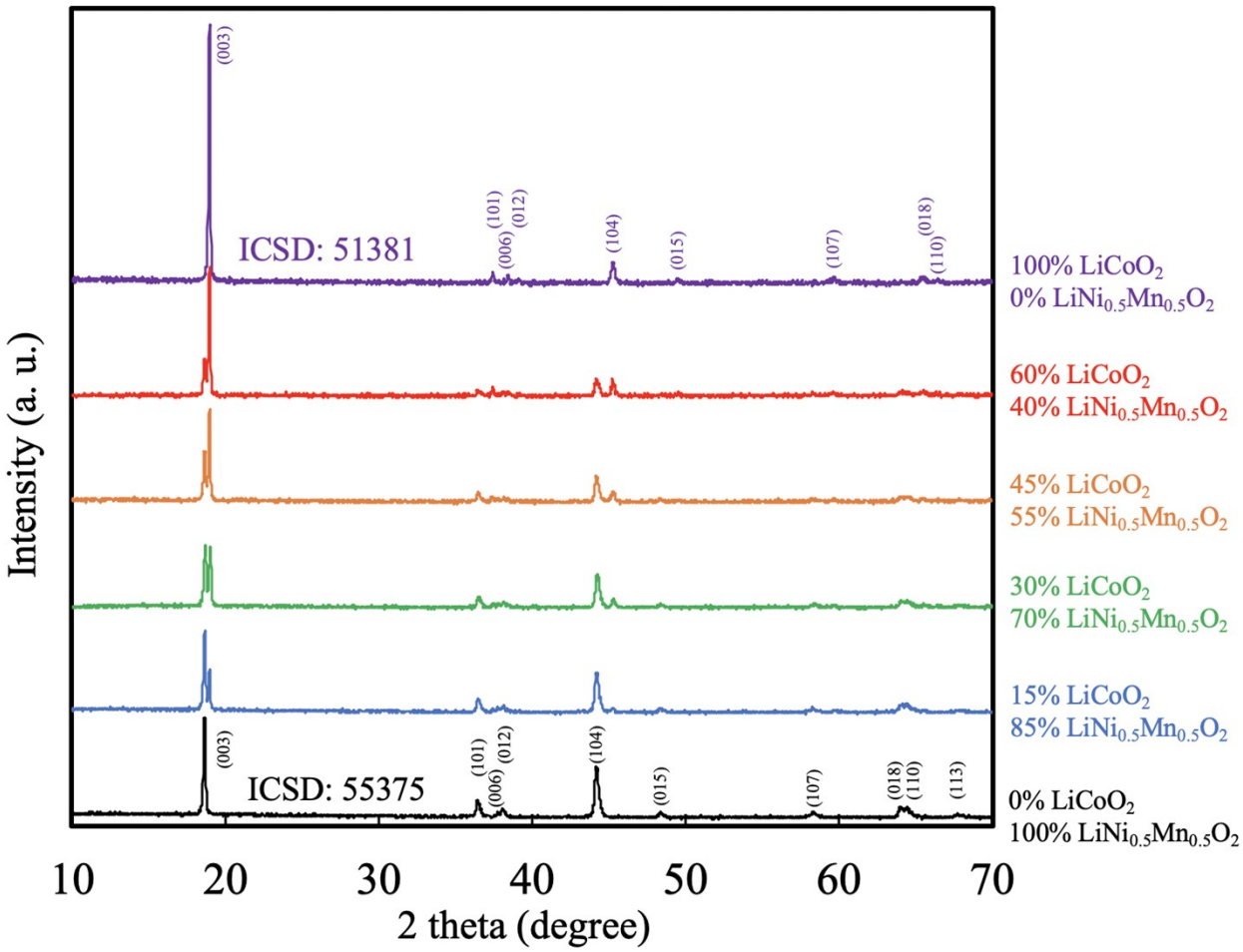

Figure S4. XRD patterns for AAM electrode pellets. The materials were 100%LCO (purple), 60%LCO (red), 45%LCO (orange), 30%LCO (green), 15%LCO (blue), and 0%LCO (black).

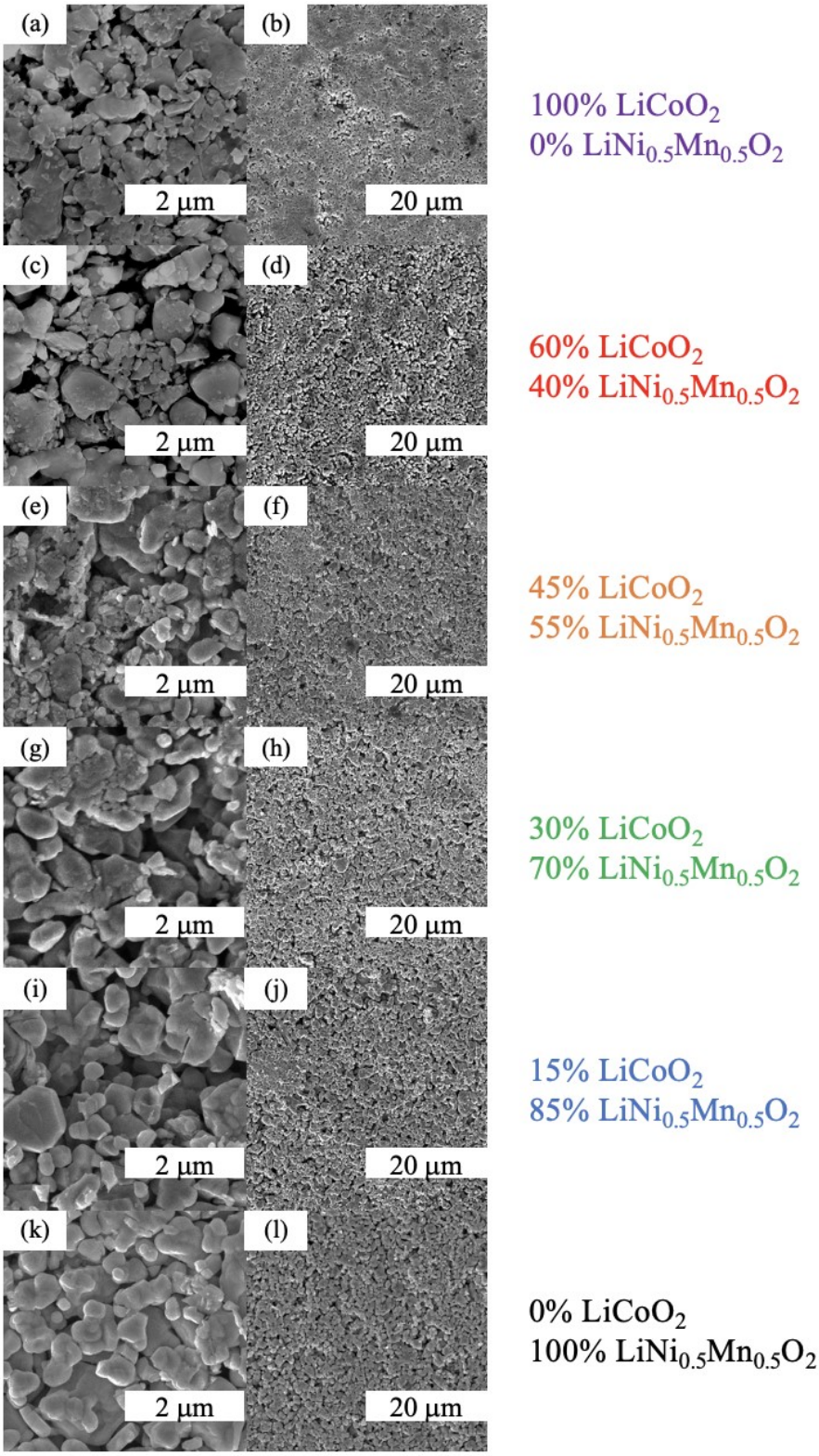

Figure S5. SEM images at relatively high magnification (left column) and low magnification (right column) taken on the surfaces of AAM electrode pellets. The relevant materials were 100%LCO (a, b), 60%LCO (c, d), 45%LCO (e, f), 30%LCO (g, h), 15%LCO (i, j), and 0%LCO (k, l).

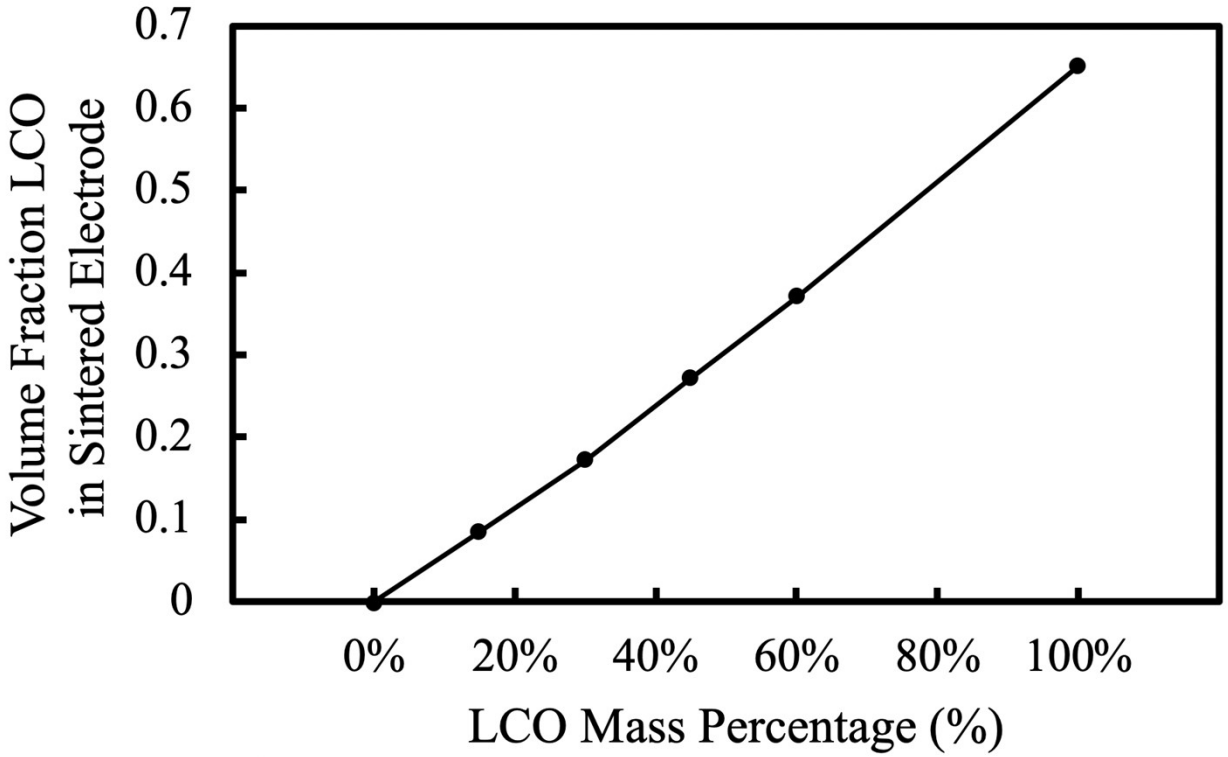

Figure S6. Volume fraction of the AAM electrode which was occupied by $LiCoO_2$ (LCO) particles as a function of LCO relative mass loading, based on the measured volume of the electrode, the measured mass of LCO in the electrode, and the crystal density of LCO.

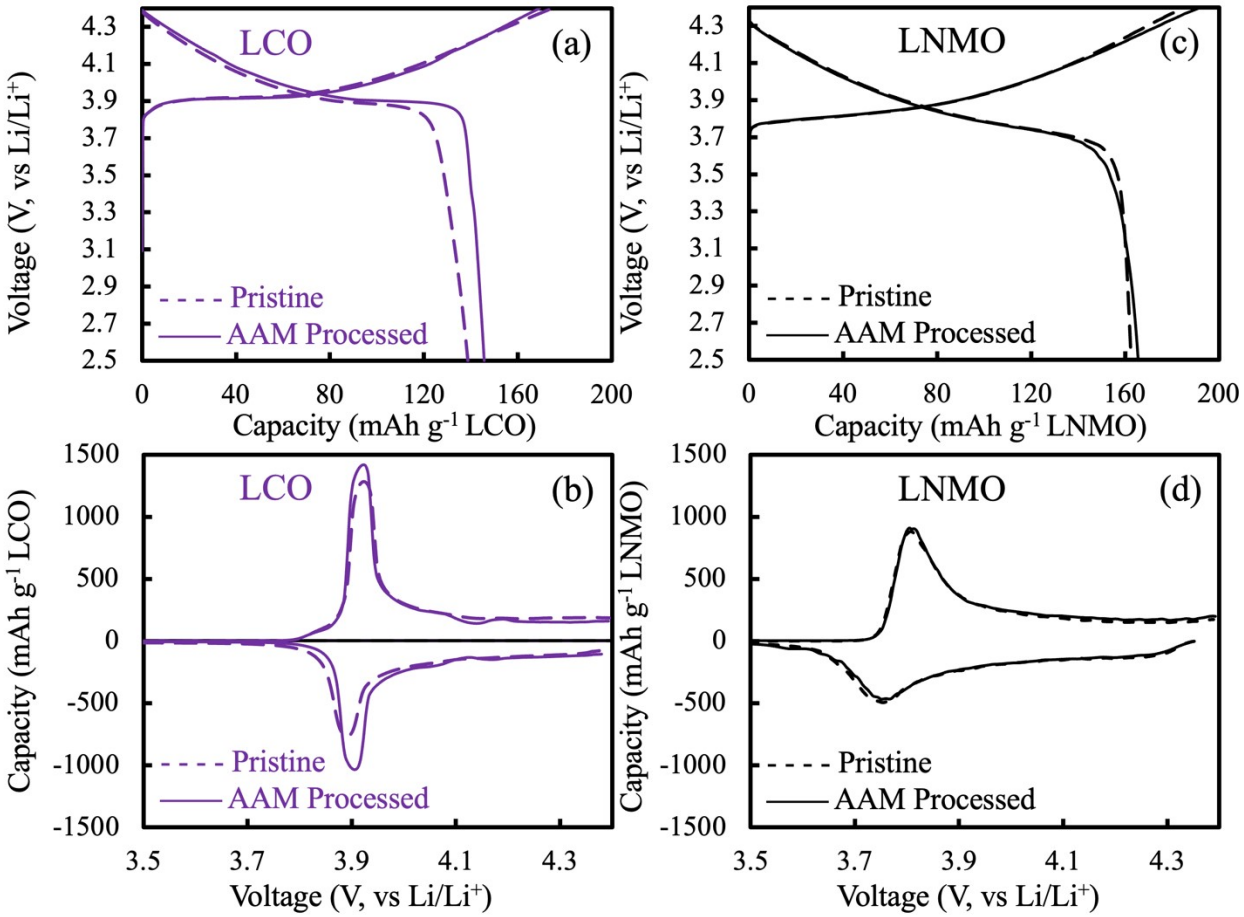

Figure S7. First cycle charge/discharge voltage profiles for (a) LCO and (c) LNMO and corresponding dQ/dV plots for (b) LCO and (d) LNMO processed into conventional composite electrodes and cycled at C/10 after pairing with Li foil anodes. The solid and dashed curve represent the as-synthesized powder and AAM treated powder. "AAM treated" powder refers to the material undergoing ethanol contact and thermal treatment as is done with AAM electrodes, although there is not hydraulic compression and the resulting powder was processed into a composite electrode.

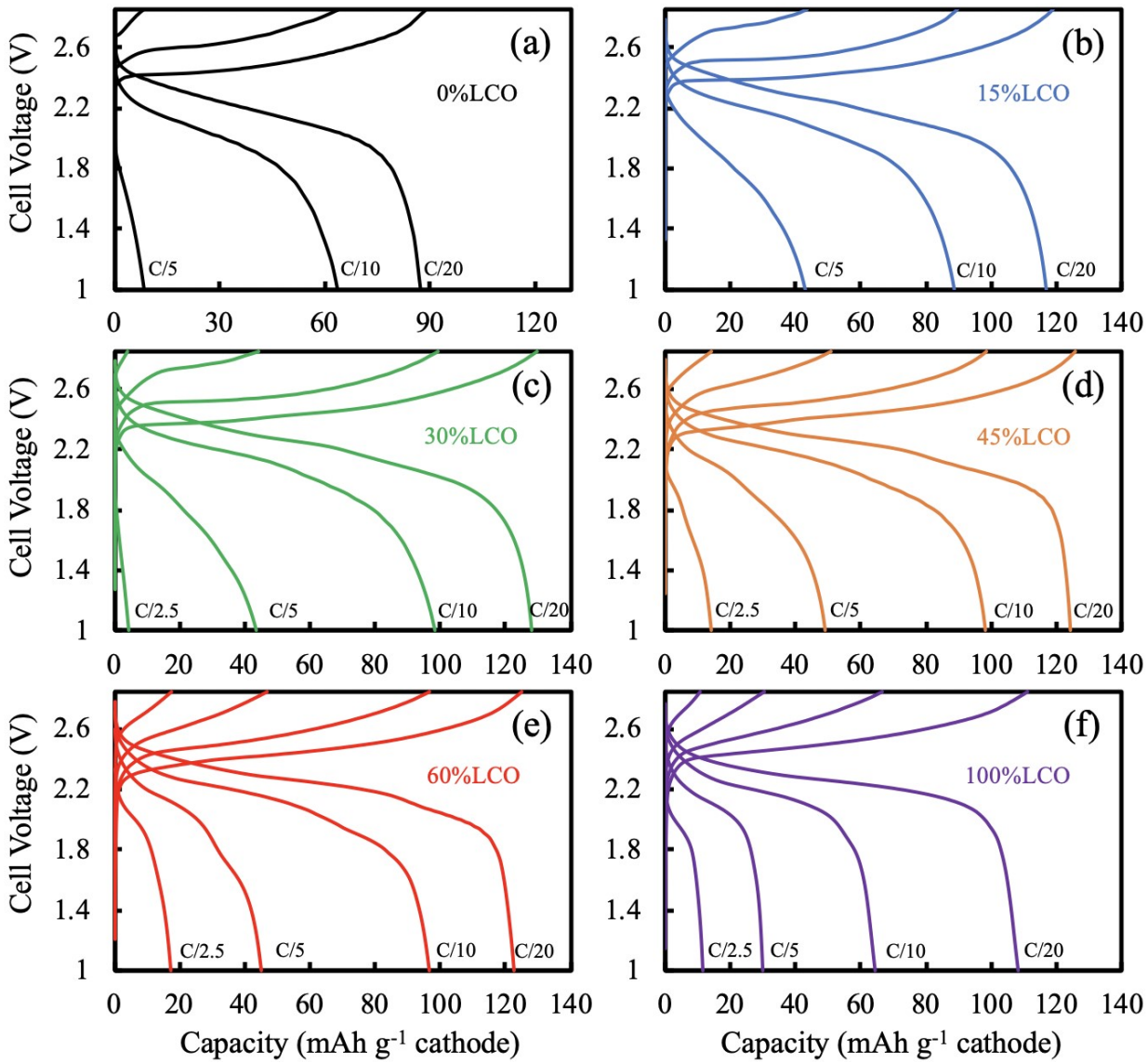

Figure S8. Voltage profiles at C/20 – C/2.5 for AAM electrode cells comprised of LTO anodes and cathodes of the composition (a) 0%LCO, (b) 15%LCO, (c) 30%LCO, (d) 45%LCO, (e) 60%LCO, and (f) 100%LCO. Charge and discharge were always performed at the same rate as indicated on the plot. For reference C/20 corresponded to ~1.13 mA cm^{-2}.

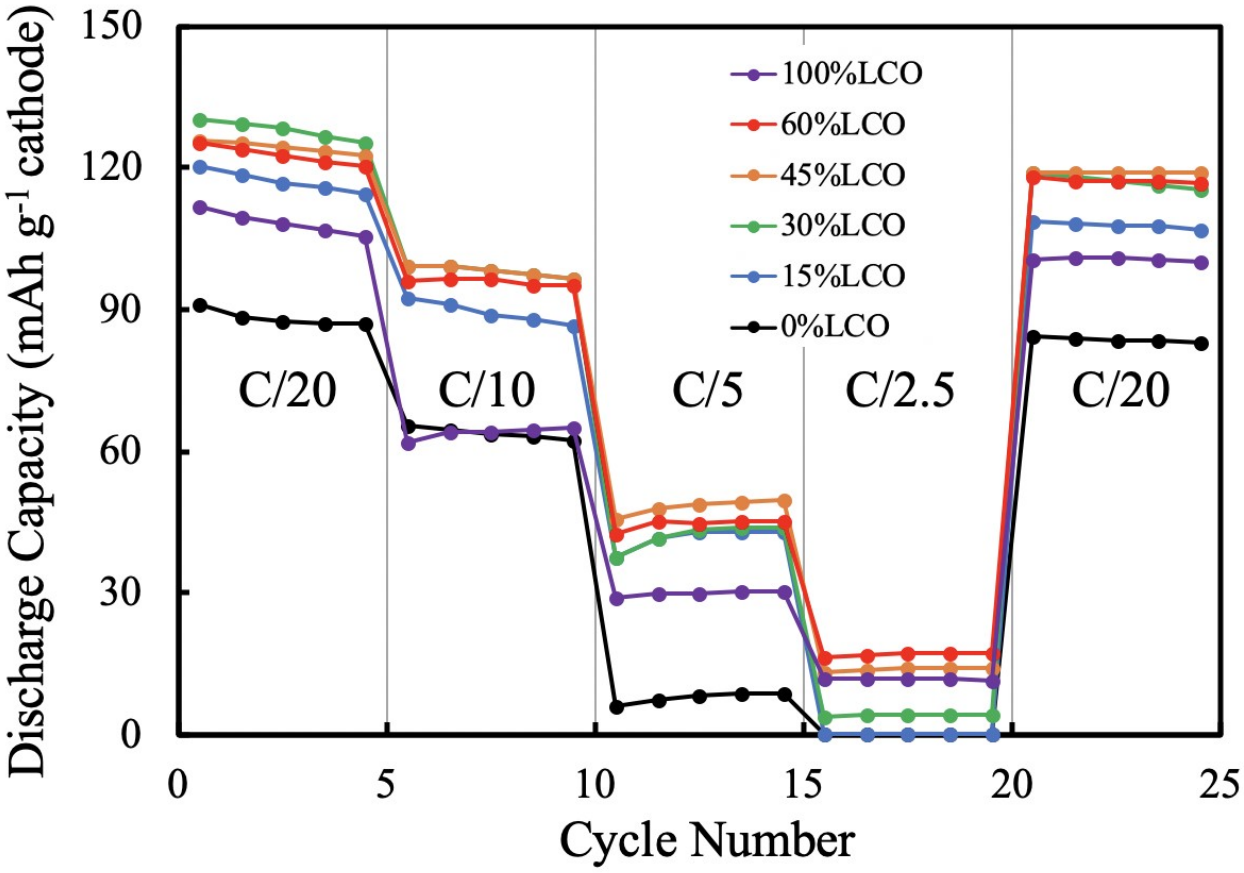

Figure S9. Discharge capacity during rate capability evaluations for AAM electrode cells with LTO anodes and cathodes with composition of 0%LCO (black), 15%LCO (blue), 30%LCO (green), 45%LCO (orange), 60%LCO (red), and 100%LCO (purple). Charge and discharge were at the same rate as indicated on the plot. For reference C/20 corresponded to ~1.13 mA cm^{-2}.

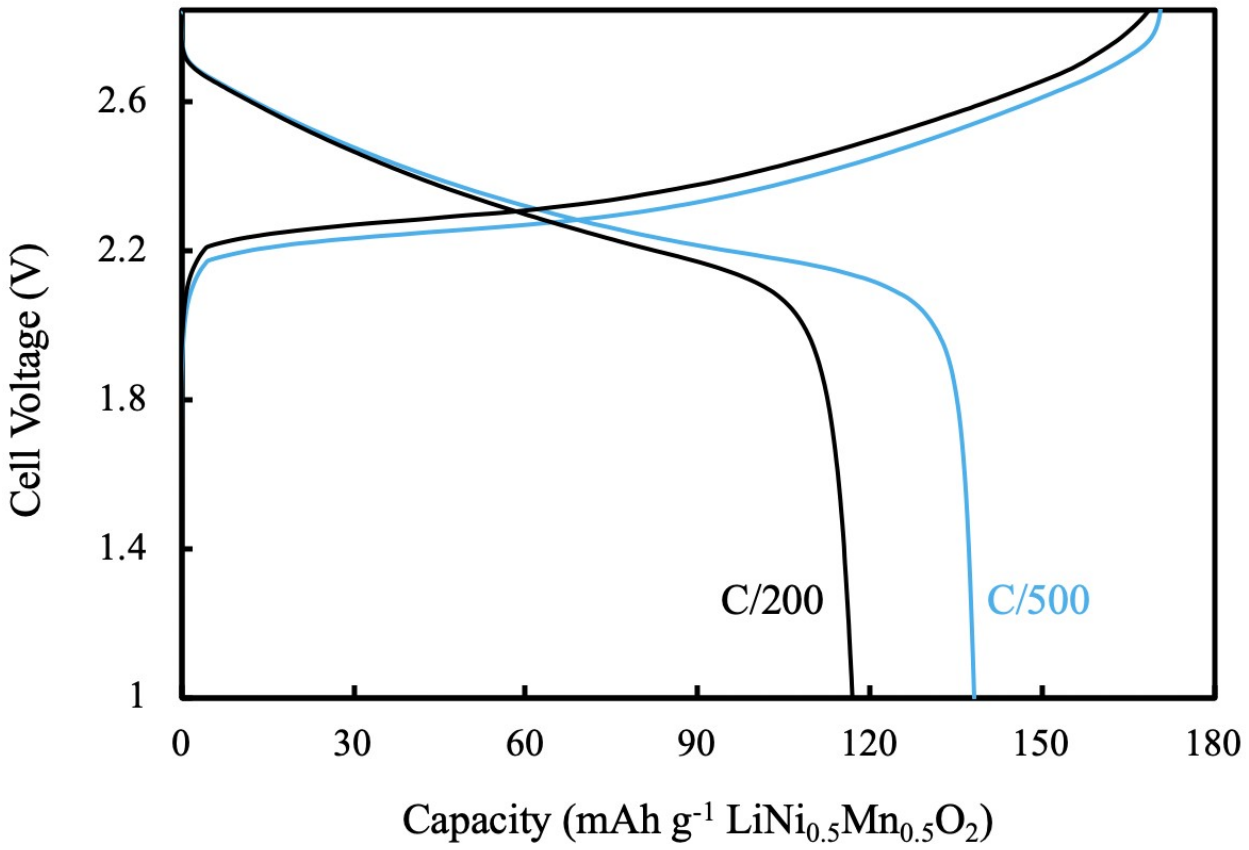

Figure S10. First cycle charge/discharge voltage profiles for 0%LCO (e.g., $LiN_{i0.5}Mn_{0.5}O_2$) using a rate of C/500 (blue) and C/200 (black) and paired with a AAM LTO anode. C/500 corresponded to 0.045 mA cm^{-2}.

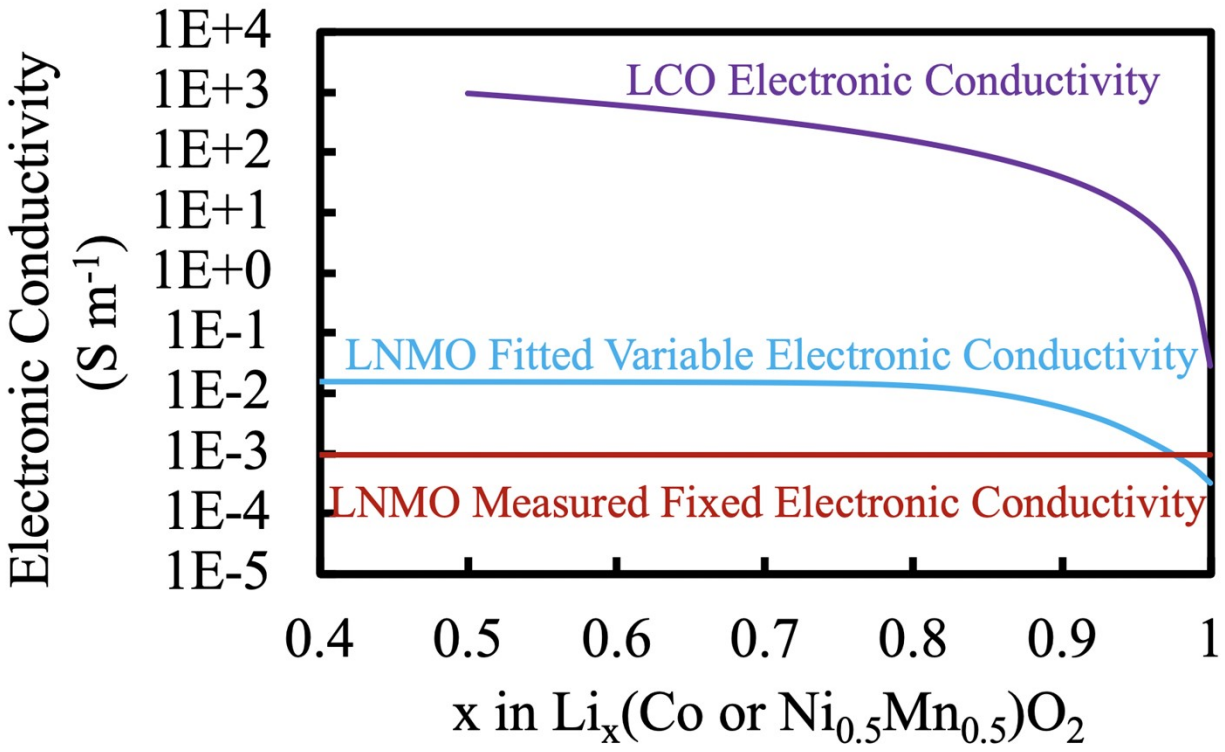

Figure S11. Electronic conductivities as a function of lithiation used in simulations. $LiCoO_2$ (LCO) electronic conductivity as a function of lithiation was based on reported literature (purple) [3]. The "Fixed Electronic Conductivity" for $LiNi_{0.5}Mn_{0.5}O_2$ (LNMO, red) used a single value which was experimentally measured for initially synthesized LNMO material The "Fitted Electronic Conductivity" for LNMO (blue) assumed a conductivity function more similar to LCO, with the plateau region conductivity determined by the best match with the experimental data for AAM LNMO discharge profiles.

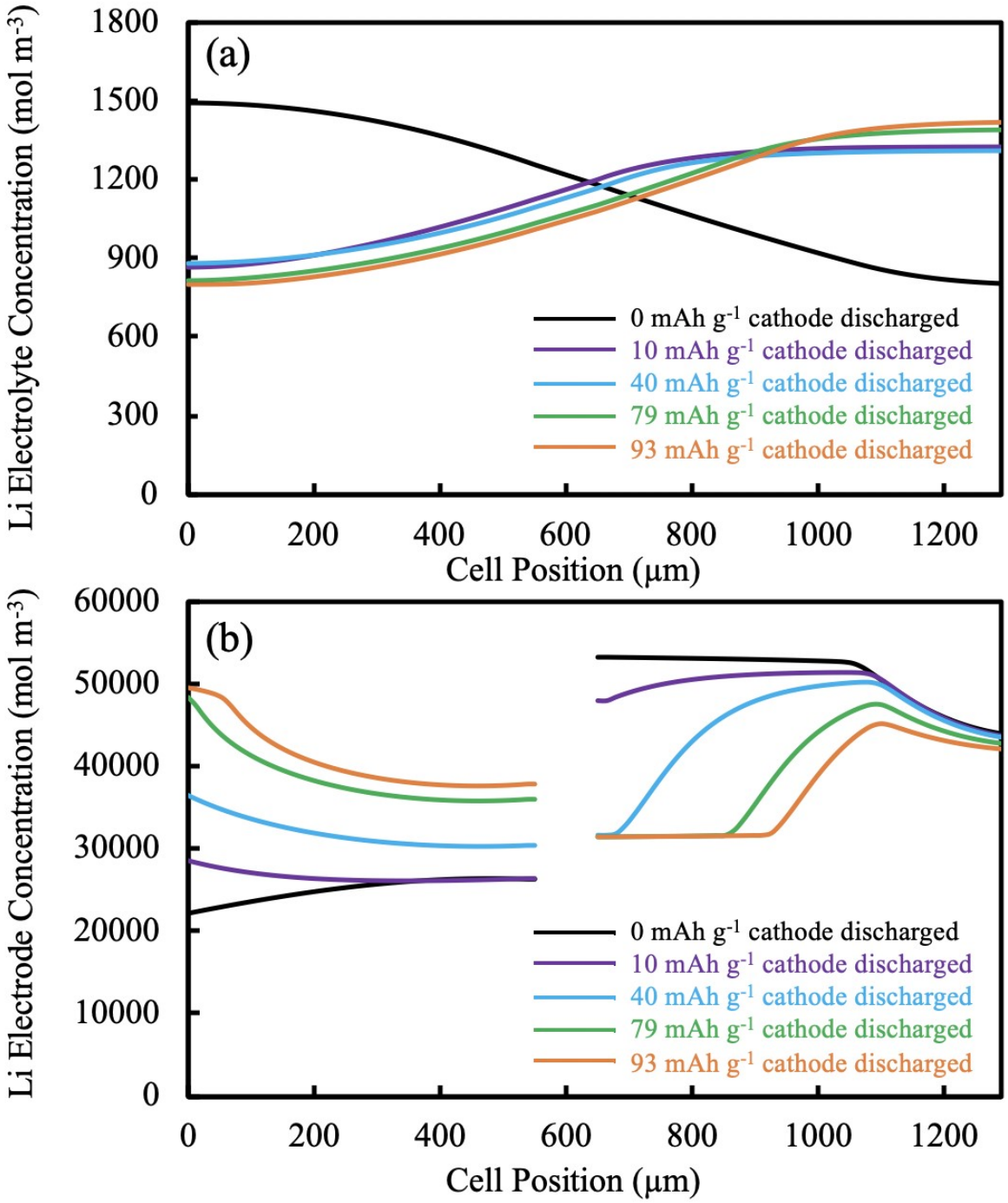

Figure S12. Simulated Li concentration in the (a) electrolyte phase and (b) solid-state electrode phase at C/20 discharge (1.13 mA cm^{-2}) following a C/20 charge cycle for pure LNMO (0%LCO) cell. Black, purple, blue, green, and orange curves represent the Li concentration at 0, 10, 40, 79, and 93 mAh g^{-1} cathode discharged. The cathode/current collector interface location is at the far left of the x-axis (e.g., "0 μm") and the anode/current collector interface is located at the maximum/far right location on the x-axis. The blank region in (b) corresponds to the separator

location (near ~600 μm), where there is not solid phase Li present but there is liquid phases/electrolyte Li.

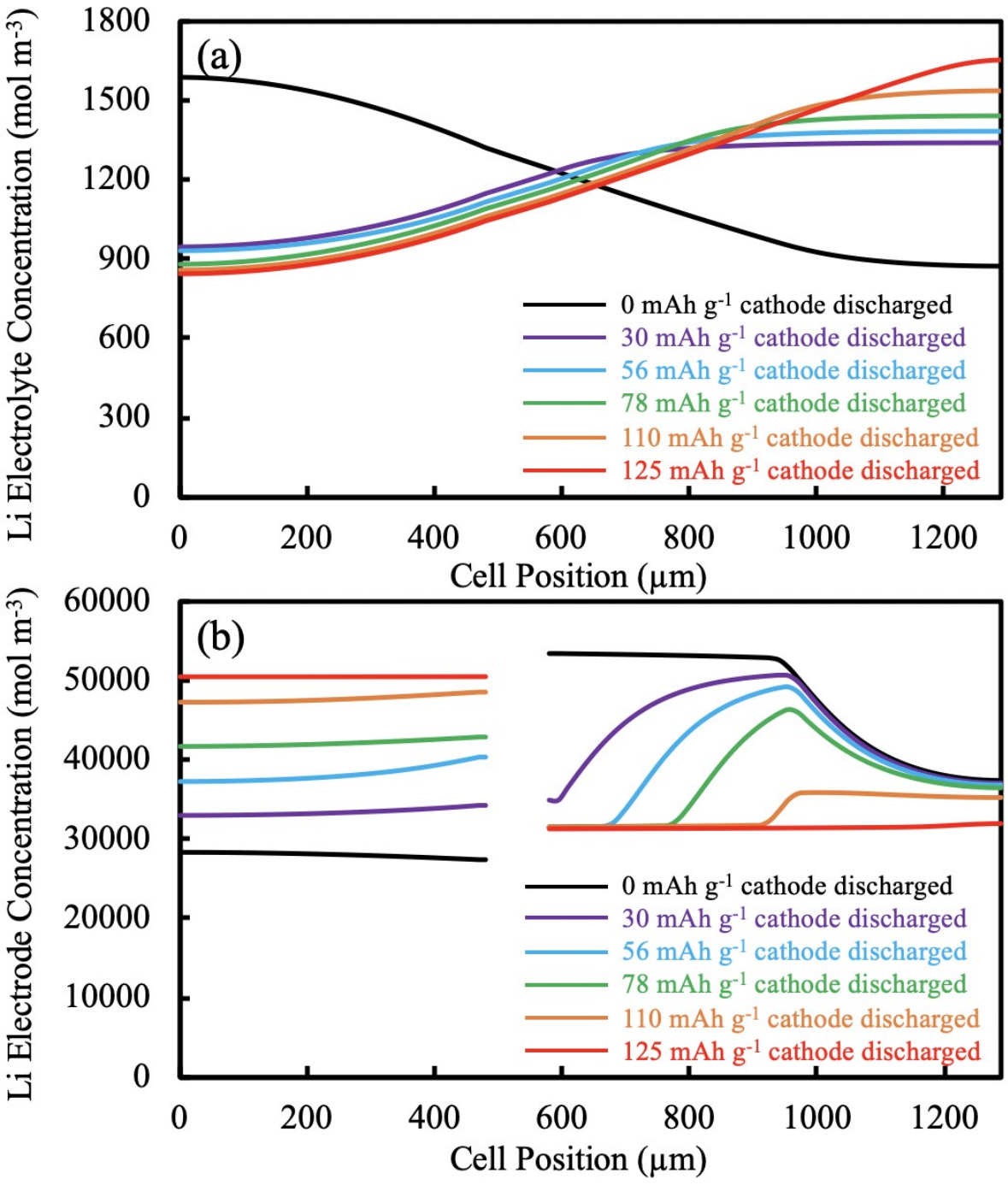

Figure S13. Simulated Li concentration in the (a) electrolyte phase and (b) electrode phase at C/20 discharge (1.13 mA cm^{-2}) following a C/20 charge cycle for 45%LCO cell. Black, purple, blue, green, orange, and red curves represent the Li concentration at 0, 30, 56, 78, 110, and 125 mAh g^{-1} cathode discharged. Cathode Li concentration is averaged by the relative mass fraction between the LNMO and LCO. The cathode/current collector interface location is at the far left of the x-axis

(e.g., "0 μm") and the anode/current collector interface is located at the maximum/far right location on the x-axis. The blank region in (b) corresponds to the separator location (near ~600 μm), where there is not solid phase Li present but there is liquid phases/electrolyte Li.

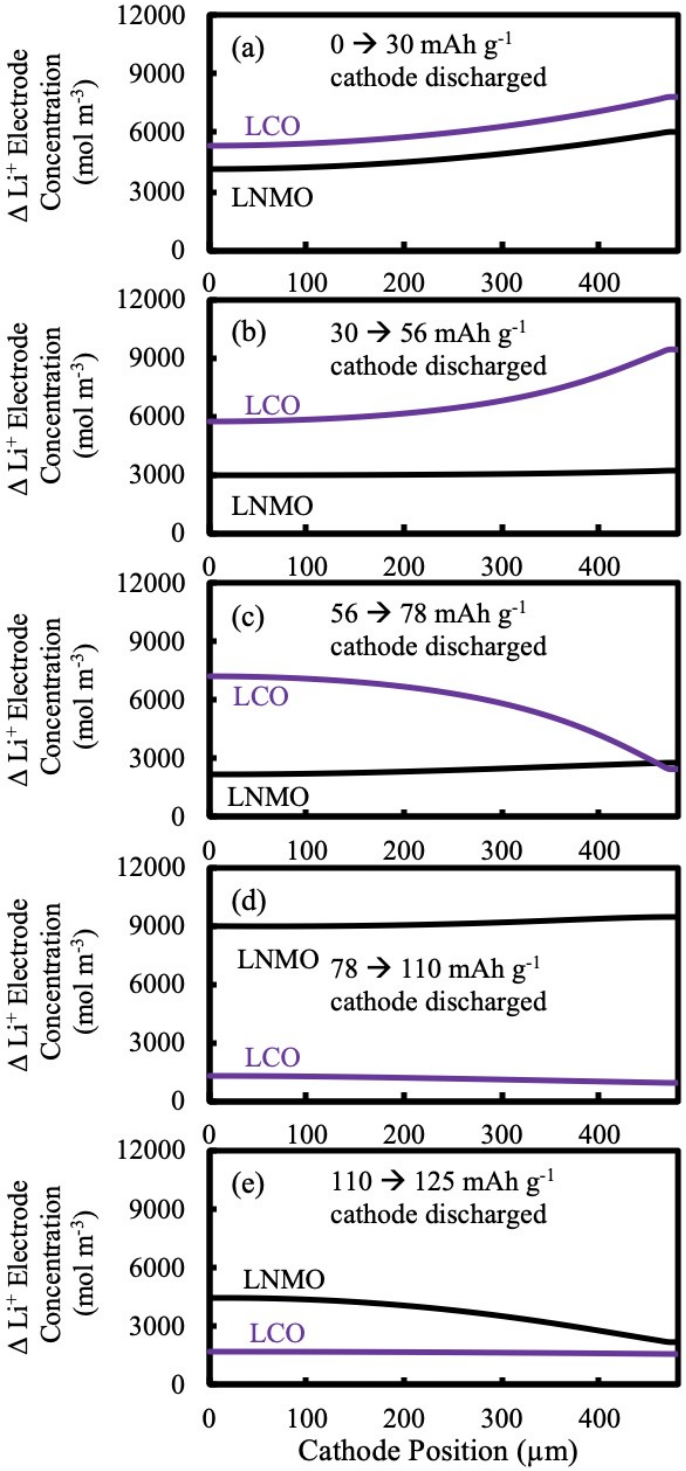

Figure S14. Simulated change in Li concentration in the LNMO (black) and LCO (purple) material as a function of position in the cathode for 45%LCO cell at different stages of discharge

at a rate of C/20 (1.13 mA cm^{-2}). The regions during discharge shown were (a) from 0 to 30 mAh g^{-1} cathode discharged, (b) from 30 to 56 mAh g^{-1} cathode discharged, (c) from 56 to 78 mAh g^{-1} cathode discharged, (d) from 78 to 110 mAh g^{-1} cathode discharged, and (e) from 110 to 125 mAh g^{-1} cathode discharged.

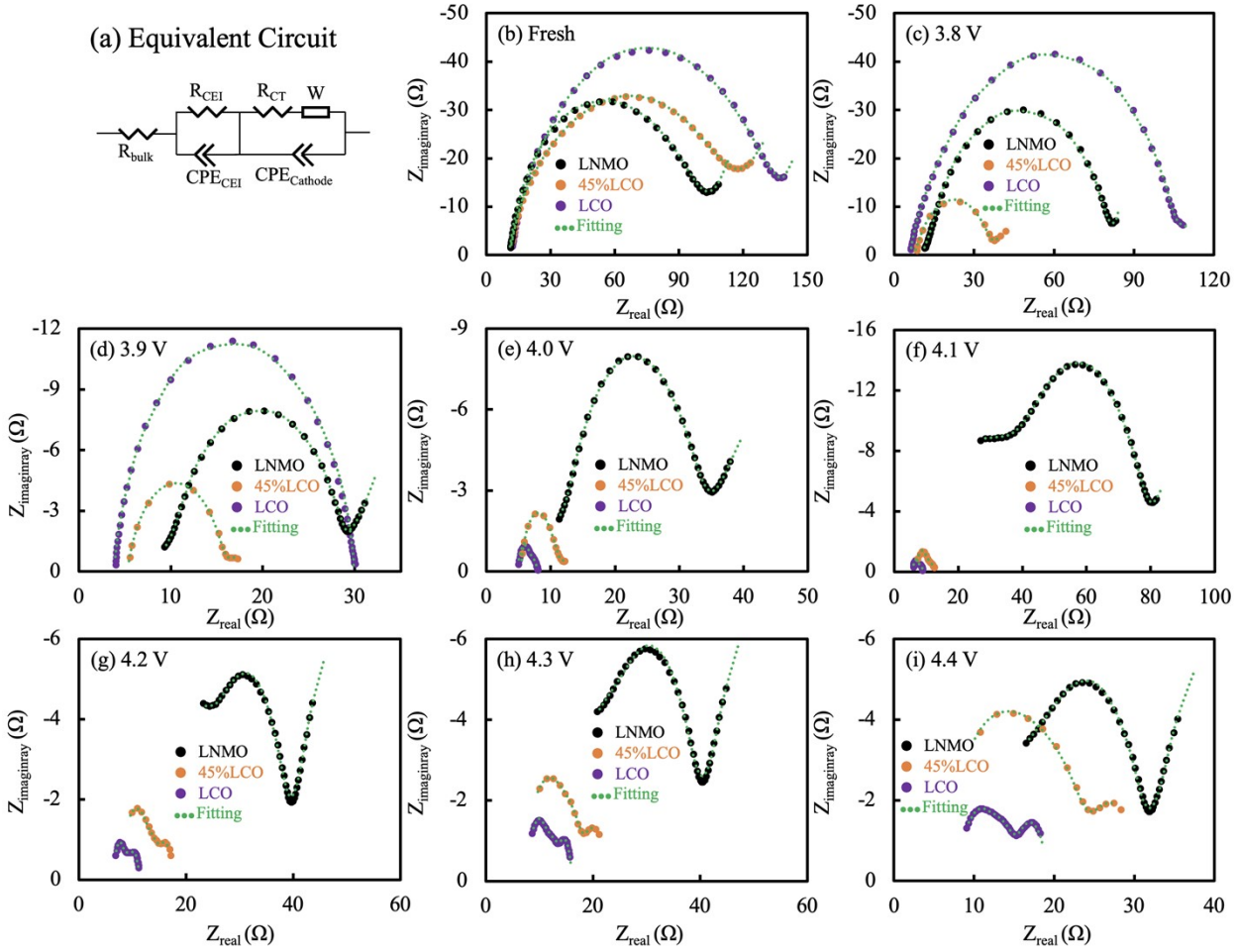

Figure S15. (a) Equivalent Circuit Model used for fitting all electrochemical impedance spectroscopy data. Nyquist plots of (b) fresh cell and after CCCV charge at (c) 3.8 V, (d) 3.9 V, (e) 4.0 V, (f) 4.1 V, (g) 4.2 V, (h) 4.3 V, and (i) 4.4 V. Black, orange, and purple dots represent LNMO, 45%LCO, and LCO, and the fitted curve were green dashed curve. The cells used AAM cathodes and lithium metal foil anodes.

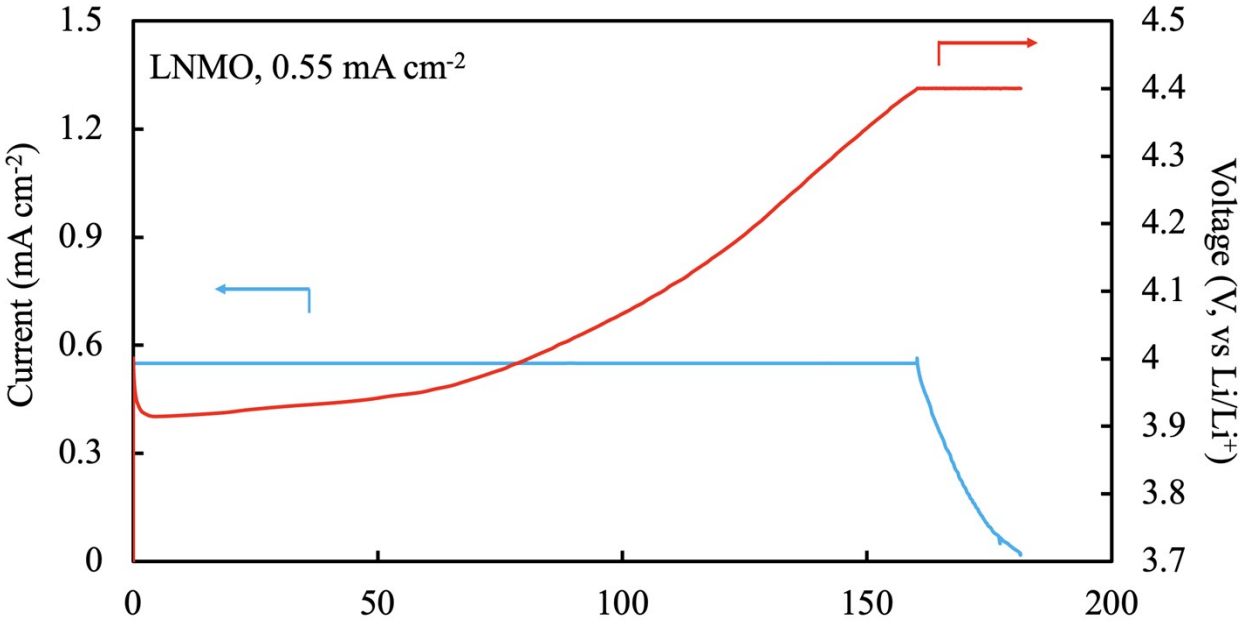

Figure S16. CCCV plot for a AAM LNMO cell paired with Li metal charged at 0.55 mA cm^{-2} and then held at 4.4 V. Red and blue curves represent the voltage and the current density, respectively.

References:

[1] M. Doyle, Comparison of Modeling Predictions with Experimental Data from Plastic Lithium Ion Cells, J. Electrochem. Soc. 143 (1996) 1890. https://doi.org/10.1149/1.1836921.

[2] T.F. Fuller, Simulation and Optimization of the Dual Lithium Ion Insertion Cell, J. Electrochem. Soc. 141 (1994) 1. https://doi.org/10.1149/1.2054684.

[3] C. Cai, Z. Nie, J.P. Robinson, D.S. Hussey, J.M. LaManna, D.L. Jacobson, G.M. Koenig, Thick Sintered Electrode Lithium-Ion Battery Discharge Simulations: Incorporating Lithiation-Dependent Electronic Conductivity and Lithiation Gradient Due to Charge Cycle, J. Electrochem. Soc. 167 (2020) 140542. https://doi.org/10.1149/1945-7111/abc747.

[4] J. Xie, N. Imanishi, T. Matsumura, A. Hirano, Y. Takeda, O. Yamamoto, Orientation dependence of Li-ion diffusion kinetics in LiCoO2 thin films prepared by RF magnetron sputtering, Solid State Ionics. 179 (2008) 362–370. https://doi.org/10.1016/j.ssi.2008.02.051.

[5] E. Zhao, M. Chen, D. Chen, X. Xiao, Z. Hu, A Versatile Coating Strategy to Highly Improve the Electrochemical Properties of Layered Oxide LiMO2 (M = Ni0.5Mn0.5 and Ni1/3Mn1/3Co1/3), ACS Appl. Mater. Interfaces. 7 (2015) 27096–27105. https://doi.org/10.1021/acsami.5b08777.

[6] B.T. Habte, F. Jiang, Microstructure reconstruction and impedance spectroscopy study of LiCoO2, LiMn2O4 and LiFePO4 Li-ion battery cathodes, Microporous Mesoporous Mater. 268 (2018) 69–76. https://doi.org/10.1016/j.micromeso.2018.04.001.

[7] H. Xia, Y.S. Meng, M.O. Lai, L. Lu, Structural and Electrochemical Properties of LiNi[sub 0.5]Mn[sub 0.5]O[sub 2] Thin-Film Electrodes Prepared by Pulsed Laser Deposition, J. Electrochem. Soc. 157 (2010) A348. https://doi.org/10.1149/1.3294719.

[8] J. Mao, W. Tiedemann, J. Newman, Simulation of Li-ion Cells by Dualfoil Model under Constant-Resistance Load, ECS Trans. 58 (2014) 71–81. https://doi.org/10.1149/05848.0071ecst.

[9] S. Venkatraman, A. Manthiram, Structural and Chemical Characterization of Layered Li1-xNi1-yMnyO2-δ (y = 0.25 and 0.5, and $0 \leq (1 - x) \leq 1$) Oxides, Chem. Mater. 15 (2003) 5003–5009. https://doi.org/10.1021/cm034757b.

[10] S. Levasseur, M. Ménétrier, E. Suard, C. Delmas, Evidence for structural defects in non-stoichiometric HT-LiCoO2: electrochemical, electronic properties and 7Li NMR studies, Solid State Ionics. 128 (2000) 11–24. https://doi.org/10.1016/S0167-2738(99)00335-5.

[11] I. Saadoune, C. Delmas, 39. The insulator – metal transition upon lithium deintercalation from, J. Mater. Chem. 9 (1999) 1135–1140.

[12] C. Cai, Z. Nie, G.M. Koenig, Multicomponent two-layered cathode for thick sintered lithium-ion batteries, Mater. Adv. (2022) 4200–4212. https://doi.org/10.1039/d1ma01074c.

[13] C. Capiglia, Y. Saito, H. Kageyama, P. Mustarelli, T. Iwamoto, T. Tabuchi, H. Tukamoto, 7Li and19F diffusion coefficients and thermal properties of non-aqueous electrolyte solutions for rechargeable lithium batteries, J. Power Sources. 81–82 (1999) 859–862. https://doi.org/10.1016/S0378-7753(98)00237-7.

[14] A. Nyman, M. Behm, G. Lindbergh, Electrochemical characterisation and modelling of the mass transport phenomena in LiPF6-EC-EMC electrolyte, Electrochim. Acta. 53 (2008) 6356–6365. https://doi.org/10.1016/j.electacta.2008.04.023.

[15] K. Zaghib, M. Simoneau, M. Armand, M. Gauthier, Electrochemical study of Li4Ti5O12 as negative electrode for Li-ion polymer rechargeable batteries, J. Power Sources. 81–82 (1999) 300–305. https://doi.org/10.1016/S0378-7753(99)00209-8.
[16] Z. Qi, G.M. Koenig, A carbon-free lithium-ion solid dispersion redox couple with low viscosity for redox flow batteries, J. Power Sources. 323 (2016) 97–106. https://doi.org/10.1016/j.jpowsour.2016.05.033.
[17] J. Chen, L. Yang, S. Fang, S.I. Hirano, K. Tachibana, Synthesis of hierarchical mesoporous nest-like Li4Ti 5O12 for high-rate lithium ion batteries, J. Power Sources. 200 (2012) 59–66. https://doi.org/10.1016/j.jpowsour.2011.10.052.
[18] K. Kataoka, Y. Takahashi, N. Kijima, J. Akimoto, K. ichi Ohshima, Single crystal growth and structure refinement of Li4Ti5O12, J. Phys. Chem. Solids. 69 (2008) 1454–1456. https://doi.org/10.1016/j.jpcs.2007.10.134.
[19] N. Nitta, F. Wu, J.T. Lee, G. Yushin, Li-ion battery materials: Present and future, Mater. Today. 18 (2015) 252–264. https://doi.org/10.1016/j.mattod.2014.10.040.
[20] D. Young, A. Ransil, R. Amin, Z. Li, Y.M. Chiang, Electronic conductivity in the Li4/3Ti5/3O 4-Li7/3Ti5/3O4 system and variation with state-of-charge as a Li battery anode, Adv. Energy Mater. 3 (2013) 1125–1129. https://doi.org/10.1002/aenm.201300134.
[21] Z. Lu, Z. Chen, J. Dahn, Lack of cation clustering in Li[NixLi1/3-2x/3Mn2/3-x/3]O-2 (0, 2 (2003) 3214–3220.
[22] M. Holzapfel, C. Haak, A. Ott, Lithium-ion conductors of the system LiCo1-xFexO2, preparation and structural investigation, J. Solid State Chem. 156 (2001) 470–479. https://doi.org/10.1006/jssc.2000.9026.